Automatica 155 (2023) 111141

Contents lists available at ScienceDirect

Automatica

journal homepage: www.elsevier.com/locate/automatica

Brief paper

Confidence set-based analysis of minimal detectable fault under hybrid Gaussian and bounded uncertainties☆

Junbo Tan [a,b], Huailiang Zheng [a], Deshan Meng [c,*], Bo Yuan [a], Xueqian Wang [a,*], Bin Liang [b]

[a] Center of Intelligent Control and Telescience, Tsinghua Shenzhen International Graduate School, 518055 Shenzhen, China
[b] Navigation and Control Research Center, Department of Automation, Tsinghua University, 100084 Beijing, China
[c] School of Aeronautics and Astronautics, Sun Yat-Sen University, Shenzhen 518107, China

ARTICLE INFO

Article history:
Received 14 October 2021
Received in revised form 31 March 2023
Accepted 15 May 2023
Available online xxxx

Keywords:
Minimal detectable fault
Hybrid uncertainties
Zonotopes

ABSTRACT

This paper proposes a confidence set-based computational method of minimal detectable fault (MDF) based on the confidence set-separation condition between the healthy and faulty residual sets for discrete linear time-invariant systems. The state-estimation-error dynamics for the analysis of MDF under hybrid random and bounded uncertainties is divided into two sub-dynamics. The first sub-dynamics is only affected by the bounded uncertainties. Under the precondition of Schur stability, an outer-approximation of minimal robust positively invariant set with any given precision is obtained. While the second sub-dynamics is only affected by the random uncertainties following the Gaussian distributions. It is proved that the behavior of the second sub-dynamics at steady stage also follows a certain Gaussian distribution, which can be bounded by confidence zonotopes given a proper confidence level. MDF for actuator and sensor faults can be obtained by solving a non-convex optimization problem to minimize the magnitude of fault subjected to the residual set-separation constraints, which is equivalent to compute a distance from the origin to hyperplane along a fixed direction by exploiting the geometric property. At the end of this paper, a two-link manipulator model and a vehicle model are used to verify the effectiveness of our proposed method.

1. Introduction

Fault diagnosis plays an important role in the safety and reliability of complex systems, which has attracted more and more attentions of researchers in the control field (Blanke et al., 2006; Patton, 1997; Zhang & Jiang, 2008). In the literature, robust fault diagnosis methods are generally divided into two categories based on the way to handle system uncertainties: the stochastic methods and the deterministic methods. The former describes system uncertainties by using stochastic distributions and the probability theory (Zhang, 2018), while the latter describes system uncertainties by using set theory (Tan et al., 2020, 2019).

The minimum detectable fault (MDF) is a typical performance index used to characterize the performance of the fault detection (FD) scheme, which also indicates the sensitivity of FD. There are also some reference literature addressing the study of MDF. Liu et al. (2005) proposed an LMI approach to minimal sensitivity analysis with application to FD based on a full characterization of the $\mathscr{H}_-$ index. Li and Zhou (2009) analyzed the problem of fault detectability from the view point of optimal filter gain of FD. In Pourasghar et al. (2016), MDF was characterized by means of residual sensitivity and invariant sets where both system inputs and uncertainties are given as unknown and bounded. Further, Kodakkadan et al. (2017) analyzed detectable sensor faults using interval observers based on two distinct approaches: invariant-sets and classical fault-sensitivity method. It is further proved from this analysis that both approaches derive distinct formulations for MDF magnitude, though qualitatively similar. Recently, Tan, Olaru, Roman, Xu and Liang (2019) established a framework to compute MDF by constructing the minimal robust positively invariant (RPI) set of linear parameter varying system based on a poly-quadratic Lyapunov function.

Although there have been some literature around the topic of MDF, the above listed works only consider the system model affected by single type of uncertainties (either random or bounded) to guarantee the robustness of computational results. Or one might consider only bounded uncertainties and capture the random uncertainties within these bounds. In general, real systems

☆ The material in this paper was not presented at any conference. This paper was recommended for publication in revised form by Associate Editor Constantino M. Lagoa under the direction of Editor Sophie Tarbouriech.

* Corresponding authors.
E-mail addresses: tjblql@sz.tsinghua.edu.cn (J. Tan), zheng.hl@sz.tsinghua.edu.cn (H. Zheng), mengdsh3@mail.sysu.edu.cn (D. Meng), boyuan@ieee.org (B. Yuan), wang.xq@sz.tsinghua.edu.cn (X. Wang), liangbin@tsinghua.edu.cn (B. Liang).

https://doi.org/10.1016/j.automatica.2023.111141
0005-1098/

could be always affected by both random and bounded uncertainties. Kofman et al. (2012) proposed the concepts of probabilistic ultimate bounds and probabilistic invariant sets to extend the notions of invariant sets and ultimate bounds to consider "containment in probability". Pizzi et al. (2019) further considered establishing a novel set-based fault tolerant control scheme for linear systems under Gaussian disturbances. Kouvaritakis et al. (2010) addressed to solve the guarantee issue of feasibility at initial time for stochastic model predictive control. Although the above works does not consider the computation problem of MDF directly, they still motivate the authors to construct invariant-set framework for linear time-invariant (LTI) systems subjected to mixed stochastic and bounded uncertainties. From the view point of reality, it is necessary to consider the computation of MDF for systems subjected to hybrid random and bounded uncertainties in order to better characterize the performance of the FD scheme. Thus, we focus on the analysis of MDF for LTI systems under hybrid Gaussian and bounded uncertainties in this context. The main contributions of this paper are summarized as follows: I. A complete framework analyzing MDF for LTI systems under hybrid Gaussian and bounded uncertainties is established based on the separation constraints of confidence residual sets in healthy and faulty situations; II. Computing MDF is formulated as a non-convex optimization problem, which is proved to be equivalent to compute a distance from the origin to hyperplane along a fixed direction.

2. Preliminaries

2.1. Notations

For a matrix $X \in \mathbb{R}^{n\times n}$, X^T, $\mathbf{tr}(X)$, $\mathbf{rank}(X)$, $\mathbf{det}(X)$ and $\mathbf{vec}(X)$ denotes the transpose, trace, rank, determinant and vectorization of X, respectively. I_n represent the identity matrix with appropriate dimensions. $\mathbf{diag}(x)$ denotes a diagonal matrix whose diagonal elements are composed of a vector $x \in \mathbb{R}^n$. $\mathbf{mat}(x)$ denotes the matrixing the vector x. $X \otimes Y$ represents the Kronecker product of matrices X and Y. For the random variables x and y, $\mathbf{E}[x]$ denotes the expectation of x. The (cross) covariance between x and y is $\mathbf{Cov}(x, y) = \mathbf{E}[(x - \mathbf{E}[x])(y - \mathbf{E}[y])^T] = \mathbf{E}[xy^T] - \mathbf{E}[x]\mathbf{E}[y]^T$. $\mathcal{P}(x \in \mathcal{D})$ is the probability that an outcome leads x to fall inside the domain $\mathcal{D}$. An n-dimensional stochastic vector x following a Gaussian probability distribution is denoted as $x \sim \mathcal{G}(\mu, Q)$, where $\mu \in \mathbb{R}^n$ and $Q \in \mathbb{R}^{n\times n}$ are the center $\mu \in \mathbb{R}^n$ and the covariance matrix $Q \in \mathbb{R}^{n\times n}$ of the Gaussian distribution, respectively. Denote the trace of the covariance matrix Q as $\mathcal{C}(Q)$. The confidence ellipsoid of x with significance level $\alpha \in (0, 1)$ can be defined as $\mathcal{E}_\alpha(\mu, Q) = \{x | x \in \mathbb{R}^n, (x - \mu)^T Q^{-1}(x - \mu) \leq \chi_n^2(1 - \alpha)\}$, where $\chi_n^2(1 - \alpha) \in \mathbb{R}$ is the value taken for probability $1 - \alpha$ by the quantile function of the chi-squared distribution with n degrees of freedom. Given two n-dimensional Gaussian distribution vectors $x \sim \mathcal{G}(\mu_x, Q_x)$, $y \sim \mathcal{G}(\mu_y, Q_y)$ and an appropriate matrix $P \in \mathbb{R}^{n\times n}$, then $x + y \sim \mathcal{G}(\mu_x + \mu_y, Q_x + Q_y)$, $Px \sim \mathcal{G}(P\mu_x, PQ_xP^T)$. The Minkowski sum of two sets X and Y is defined as $X \oplus Y = \{x + y \mid x \in X, y \in Y\}$.

2.2. Zonotopes

A zonotope Z is defined as $Z = g \oplus H\mathbb{B}^t$, where g and H are its center and generator matrix, respectively, $\mathbb{B}^t$ is an interval vector composed of t unitary intervals $[-1, 1]$. Here a zonotope is denoted as $Z = \langle g, H\rangle$ for simplicity. Given two zonotopes $Z_1 = \langle g_1, H_1\rangle$ and $Z_2 = \langle g_2, H_2\rangle$, $Z_1 \oplus Z_2 = \langle g_1 + g_2, [H_1\ H_2]\rangle$. Given a zonotope $Z = \langle g, H\rangle$ and a compatible matrix K, $KZ = \langle Kg, KH\rangle$. Given $X = \langle g_1, \alpha H\rangle$ and $Y = \langle g_2, \beta H\rangle$, where $\alpha, \beta \in \mathbb{R}^+$, then $X \oplus Y = \langle g_1 + g_2, (\alpha + \beta)H\rangle$.

Definition 2.1. For a matrix $H = [h_1, \ldots, h_i, \ldots, h_{n-1}] \in \mathbb{R}^{n\times(n-1)}$, where h_i denotes the ith column of H, then n-dimensional cross-product of H is defined as $\mathbf{nX}(H) \triangleq \left[\mathbf{det}(H^{(1)}), \ldots, (-1)^{i+1}\mathbf{det}(H^{(i)}), \ldots, (-1)^{n+1}\mathbf{det}(H^{(n)})\right]^T$, where $H^{(i)} \in \mathbb{R}^{(n-1)\times(n-1)}$ denotes a matrix where the ith row of H is removed.

Lemma 2.1. *The halfspace representation $\mathcal{H}(Z) = \{x \in \mathbb{R}^n | \mathcal{A}x \leq \mathcal{B}\}$ of a zonotope $Z = \langle g, H\rangle \subseteq \mathbb{R}^n$ with $H = [h_1, \ldots, h_m] \in \mathbb{R}^{n\times m}$ is*

$$\mathcal{A} = \begin{bmatrix} \mathcal{A}^+ & -\mathcal{A}^+ \end{bmatrix}^T, \mathcal{B} = \begin{bmatrix} \mathcal{B}^+ & \mathcal{B}^- \end{bmatrix}^T,$$

$$\mathcal{A}_s^+ = \frac{\mathbf{nX}(H^{\langle\gamma,\ldots,\eta\rangle})^T}{\|\mathbf{nX}(H^{\langle\gamma,\ldots,\eta\rangle})\|_2}, \mathcal{B}_s^+ = \mathcal{A}_s^+ g + \Delta\mathcal{B}_s,$$

$$\mathcal{B}_s^- = -\mathcal{A}_s^+ g + \Delta\mathcal{B}_s, \Delta\mathcal{B}_s = \sum_{j=1}^{m} |\mathcal{A}_s^+ h_j|.$$

$\mathcal{A}_s^+$, $\mathcal{B}_s^+$ and $\mathcal{B}_s^-$ denote the sth rows of $\mathcal{A}^+$, $\mathcal{B}^+$ and $\mathcal{B}^-$, respectively. The index s varies from 1 to $\binom{m}{n-1}$ and the indices $\gamma, \ldots, \eta$ are obtained by picking $n - 1$ out of m elements. $H^{\langle\gamma,\ldots,\eta\rangle}$ denotes matrix H where the columns indexed by $\gamma, \ldots, \eta$ are removed.

More details on matrix calculus, probability distributions, ellipsoids and zonotopes can be referred to Alamo et al. (2005), Althoff (2010), Byod and Vandenberghe (2004), Combastel (2015) and Zhang (2016).

3. System models

3.1. Plant model

The discrete linear time-invariant system under the effect of additive actuator and sensor faults is modeled as the following form:

$$x_{k+1} = Ax_k + Bu_k + Gf_k + E_z w_{z,k} + E_g w_{g,k}, \tag{1a}$$

$$y_k = Cx_k + Ps_k + F_z v_{z,k} + F_g v_{g,k}, \tag{1b}$$

where $x_k \in \mathbb{R}^{n_x}$, $u_k \in \mathbb{R}^{n_u}$ and $y_k \in \mathbb{R}^{n_y}$ denote the state, input and output of system at time instant k. $w_{z,k} \in \mathbb{R}^{n_{wz}}$ and $v_{z,k} \in \mathbb{R}^{n_{vz}}$ represent the set-bounded disturbance and measurement error, respectively. $w_{g,k} \in \mathbb{R}^{n_{wg}}$ and $v_{g,k} \in \mathbb{R}^{n_{vg}}$ represent Gaussian disturbance and measurement noise, respectively. All the uncertainties are mutually independent. $f_k \in \mathbb{R}^{n_f}$ and $s_k \in \mathbb{R}^{n_s}$ denote the additive actuator and sensor fault vectors, respectively. $A \in \mathbb{R}^{n_x\times n_x}$, $B \in \mathbb{R}^{n_x\times n_u}$, $E_z \in \mathbb{R}^{n_x\times n_{wz}}$, $E_g \in \mathbb{R}^{n_x\times n_{wg}}$, $C \in \mathbb{R}^{n_y\times n_x}$, $F_z \in \mathbb{R}^{n_y\times n_{vz}}$, $F_g \in \mathbb{R}^{n_y\times n_{vg}}$, $G \in \mathbb{R}^{n_x\times n_f}$ and $P \in \mathbb{R}^{n_y\times n_s}$ are constant matrices with appropriate dimensions. It is assumed that the disturbance $w_{z,k}$ and the measurement error $v_{z,k}$ are bounded by given zonotopes: $w_{z,k} \in \mathbf{W}_z = \langle w_z^c, H_w\rangle$, $v_{z,k} \in \mathbf{V}_z = \langle v_z^c, H_v\rangle$, where w_z^c, v_z^c, H_w and H_v are given constant vectors and matrices. Similarly, the stochastic disturbance $w_{g,k}$ and the measurement noise $v_{g,k}$ are assumed to obey the following Gaussian distributions: $w_{g,k} \sim \mathcal{G}(w_g^c, Q_w)$, $v_{g,k} \sim \mathcal{G}(v_g^c, Q_v)$, where w_g^c, v_g^c, Q_w and Q_v are given constant vectors and matrices.

3.2. Design of FD observer

In order to implement robust FD, we construct the following Luenberger-structure observer:

$$\hat{x}_{k+1} = A\hat{x}_k + Bu_k + L(y_k - \hat{y}_k), \tag{2a}$$

$$\hat{y}_k = C\hat{x}_k, \tag{2b}$$

where $\hat{x}_k$ and $\hat{y}_k$ are the estimated state and output vectors of the system (1), respectively. $L \in \mathbb{R}^{n_x\times n_y}$ is the gain matrix of the

designed FD observer (2). In the healthy situation without any actuator or sensor fault (i.e., $f = 0, g = 0$), the state-estimation error e_k and the residual r_k are defined as

$$e_k = x_k - \hat{x}_k, \tag{3a}$$

$$r_k = y_k - \hat{y}_k, \tag{3b}$$

respectively. Furthermore, by combining (1a) and (2a), the dynamics of the state-estimation error e_k in the healthy situation is obtained as

$$\begin{aligned} e_{k+1} =&(A - LC)e_k + E_z w_{z,k} + E_g w_{g,k} \\ &- LF_z v_{z,k} - LF_g v_{g,k}. \end{aligned} \tag{4}$$

The corresponding residual r_k is rewritten as

$$r_k = Ce_k + F_z v_{z,k} + F_g v_{g,k}. \tag{5}$$

For the convenience of analysis, we split the dynamics (4) of e_k into the following two sub-dynamics:

$$e_{z,k+1} =(A - LC)e_{z,k} + E_z w_{z,k} - LF_z v_{z,k}, \tag{6a}$$

$$e_{g,k+1} =(A - LC)e_{g,k} + E_g w_{g,k} - LF_g v_{g,k}, \tag{6b}$$

and it follows $e_k = e_{z,k} + e_{g,k}$. Furthermore, the residual r_k in (5) is rewritten as

$$r_k = r_{z,k} + r_{g,k}, \tag{7a}$$

$$r_{z,k} = Ce_{z,k} + F_z v_{z,k}, \tag{7b}$$

$$r_{g,k} = Ce_{g,k} + F_g v_{g,k}. \tag{7c}$$

4. Dynamics analysis in healthy/faulty situations

4.1. Dynamics analysis in healthy situation

As for (6a), if there exists gain matrix $L \in \mathbb{R}^{n_x \times n_y}$ such that $A - LC$ is a Schur matrix, then, there exist a family of RPI sets for the dynamics (6a) (Blanchini, 1999). Based on the results in Tan, Olaru, Roman, Xu and Liang (2019), we can obtain the minimal RPI (mRPI) set $\mathbf{E}_{z,\infty} = \sum_{i=0}^{\infty}(A - LC)^i(E_z\mathbf{W}_z \oplus (-LF_z)\mathbf{V}_z)$ and its outer-approximation $\mathbf{E}_z$ with any given precision for the dynamics (6a). For the convenience of analysis, with a little abuse of notation, we will use the outer-approximation set to replace the mRPI set in the subsequent context. Note that, in principle, $\mathbf{E}_z$ can be chosen to approximate the mRPI set $\mathbf{E}_{z,\infty}$ with any given precision in advance. Thus, the error and conservatism introduced for FD by using $\mathbf{E}_z$ to replace $\mathbf{E}_{z,\infty}$ can be ignored. Furthermore, for the residual $r_{z,k}$ in (7b), at the steady stage, it follows

$$r_{z,\infty} \in \mathbf{R}_z = C\mathbf{E}_z \oplus F_z\mathbf{V}_z. \tag{8}$$

Based on the above analysis, it is found that the residual set $\mathbf{R}_z$ could be computed off-line. For brevity, we denote $\mathbf{R}_z$ by $\langle r_z^c, H_z\rangle$, i.e., $\mathbf{R}_z = \langle r_z^c, H_z\rangle$.

Theorem 4.1. *Under the Schur stability on $A - LC$, the state-estimation error $e_{g,\infty}$ at steady stage follows the Gaussian distribution: $e_{g,\infty} \sim \mathcal{G}(\beta_\infty, \Phi_\infty)$, and*

$$\beta_\infty = (I - A + LC)^{-1}(E_g w_g^c - LF_g v_g^c), \tag{9a}$$

$$\begin{aligned} \Phi_\infty = \mathbf{mat}&[(I - (A - LC) \otimes (A - LC))^{-1} \\ &\mathbf{vec}(E_g Q_w E_g^T + LF_g Q_v F_g^T L^T)]. \end{aligned} \tag{9b}$$

Please see the Appendix for the proof. □

Based on Theorem 4.1, considering $v_{g,k} \sim \mathcal{G}(v_g^c, Q_v), \forall k \in \mathbb{N}^+$, $r_{g,k}$ in (7c) also follows the Gaussian distribution at steady stage as

$$r_{g,\infty} \sim \mathcal{G}(C\beta_\infty + F_g v_g^c, C\Phi_\infty C^T + F_g Q_v F_g^T). \tag{10}$$

Further, as $k \to \infty$, we have from (7a) that

$$r_\infty = r_{z,\infty} + r_{g,\infty}. \tag{11}$$

4.2. Dynamics analysis in faulty situation

In this subsection, we mainly consider single actuator-fault situation to compute the magnitude of MDF for each fault f_i, where f_i is the ith component of f_k corresponding to the ith actuator fault. In this case, the analysis is carried on the following actuator-fault dynamics:

$$x_{k+1} =Ax_k + Bu_k + G_i f_i + E_z w_{z,k} + E_g w_{g,k}, \tag{12a}$$

$$y_k =Cx_k + F_z v_{z,k} + F_g v_{g,k}, \tag{12b}$$

where G_i denotes the ith column of G. For simplicity, here we mainly consider the case of $f_i > 0$. The situation $f_i < 0$ can be handled similarly using an equivalent transformation $G_i f_i = -G_i(-f_i)$. By combining (12) and the observer (2), the state-estimation-error dynamics affected by the ith actuator fault is obtained as

$$\begin{aligned} e_{k+1}^{a,i} =&(A - LC)e_k^{a,i} + G_i f_i + E_z w_{z,k} + E_g w_{g,k} \\ &- LF_z v_{z,k} - LF_g v_{g,k}, \end{aligned} \tag{13}$$

Similar to the dealing way in the healthy situation, the state-estimation error $e_k^{a,i}$ is also split into three parts $e_{z,k}$, $e_{g,k}$ and $e_{f,k}^{a,i}$, i.e., $e_k^{a,i} = e_{f,k}^{a,i} + e_{z,k} + e_{g,k}$. The dynamics of $e_{z,k}$ and $e_{g,k}$ have been derived in (6), while the dynamics of $e_{f,k}^{a,i}$ is given as

$$e_{f,k+1} = (A - LC)e_{f,k}^{a,i} + G_i f_i. \tag{14}$$

Obviously, at steady stage, it follows

$$e_{f,\infty}^{a,i} = (I - A + LC)^{-1} G_i f_i. \tag{15}$$

Based on the dynamics (13), the residual $r_k^{a,i}$ under the ith actuator fault is obtained as

$$\begin{aligned} r_k^{a,i} =&Ce_k^{a,i} + F_z v_{z,k} + F_g v_{g,k} \\ =&Ce_{f,k}^{a,i} + r_{z,k} + r_{g,k}. \end{aligned} \tag{16}$$

By letting $k \to \infty$, it follows

$$r_\infty^{a,i} = C(I - A + LC)^{-1} G_i f_i + r_{z,\infty} + r_{g,\infty}. \tag{17}$$

5. Computing MDF for actuators

Since the random vector $r_{g,\infty}$ in (10) follows the Gaussian distribution such that the support of $r_{g,\infty}$ is unbounded. Thus, the supports of the real residual vector r_∞ and $r_\infty^{a,i}$ are also all unbounded based on (11) and (17). In order to compute the confidence set-based MDF, the following theorem first gives the confidence zonotope for the random vector $r_{g,\infty}$.

Theorem 5.1 (*Confidence Zonotope*)**.** *For the random vector $r_{g,\infty}$ in (10), let $\alpha \in [0, 1]$ and the confidence zonotope $\mathbf{R}_g = \langle \mu, \sqrt{\chi_n^2(1-\alpha)}S^{-1}\Lambda^{\frac{1}{2}}\rangle$, where $\mu = C\beta_\infty + F_g v_g^c$. S and Λ satisfy the orthogonal decomposition of the real symmetric matrix $C\Phi_\infty C^T + F_g Q_v F_g^T$, i.e., $C\Phi_\infty C^T + F_g Q_v F_g^T = S^T \Lambda S$. $\Lambda^{\frac{1}{2}}$ denotes a diagonal matrix whose diagonal elements are the square root of the diagonal elements of Λ. Then, $\mathcal{P}(r_{g,\infty} \in \mathbf{R}_g) \geq 1 - \alpha$.*

Please see the Appendix for the proof. □

Remark 5.1. Without considering the calculation cost, it is possible to consider using an iterative algorithm to find a zonotope to approximate the ellipsoid with higher accuracy (Chabane et al., 2014; Gaßmann & Althoff, 2020). Although an analytical solution is given in Theorem 5.1, the approximation precision of this method is lower than that of the iterative algorithm.

Based on Theorem 5.1, we can use the confidence zonotope $\mathbf{R}_g$ of the random vector $r_{g,\infty}$ to construct the confidence residual sets $\mathbf{R}$ and $\mathbf{R}^{a,i}$ for the residual vectors r_∞ and $r_\infty^{a,i}$, respectively. Considering $r_{z,\infty} \in \mathbf{R}_z$, (11) and (17), we construct $\mathbf{R}$ and $\mathbf{R}^{a,i}$ as

$$\mathbf{R} = \mathbf{R}_z \oplus \mathbf{R}_g, \tag{18a}$$

$$\mathbf{R}^{a,i} = \{C(I - A + LC)^{-1} G_i f_i\} \oplus \mathbf{R}_z \oplus \mathbf{R}_g. \tag{18b}$$

Theorem 5.2. *For the confidence residual sets* $\mathbf{R}$ *and* $\mathbf{R}^{a,i}$*, it follows*

$$\mathcal{P}(r_\infty \in \mathbf{R}) \geq 1 - \alpha, \tag{19a}$$

$$\mathcal{P}(r_\infty^{a,i} \in \mathbf{R}^{a,i}) \geq 1 - \alpha. \tag{19b}$$

Please see the Appendix for the proof. □

The monitoring criterion for FD based on confidence residual sets at steady stage needs to real-timely check whether $r_k \in \mathbf{R}$ holds or not. If $r_k \notin \mathbf{R}$, it indicates that the system (1) is faulty at time instant k. Otherwise, we still consider that the system (1) operates in the healthy situation. Once actuator fault occurs in the system (1), it is known that the residual signal r_k will converge towards the confidence residual set $\mathbf{R}^{a,i}$. Therefore, as long as the intersection of the healthy residual set $\mathbf{R}$ and the actuator-fault residual set $\mathbf{R}^{a,i}$ is empty, i.e., $\mathbf{R} \cap \mathbf{R}^{a,i} = \emptyset$, it can be guaranteed the occurred actuator fault will be detected at the steady stage with the confidence level $1-\alpha$ based on Theorem 5.2. Thus, in order to compute the magnitude of MDF for actuators, we formulate the following optimization problem:

$$\min_{f_i > 0} f_i \quad \text{s.t. } \mathbf{R} \cap \mathbf{R}^{a,i} = \emptyset. \tag{20}$$

Remark 5.2. For (20), only the calculation of MDF in steady stage is considered. Although calculating the magnitude of MDF in transition stage is a difficult problem, one possible way is to use the set-valued observer method to generate a varying residual set online to compute the magnitude of MDF during the transition state.

It is not easy to directly solve the optimization problem (20) considering the non-convexity of the constraint $\mathbf{R} \cap \mathbf{R}^{a,i} = \emptyset$. Solving the non-convex optimization problem (20) is equivalently transformed into computing the distance from the origin to hyperplane along a fixed direction, which is detailedly illustrated in the following theorem.

Theorem 5.3. *The optimal solution* f_i^* *for the optimization problem* (20) *can be given as*

$$f_i^* \triangleq \min\{f_i^t\},\ 1 \leq t \leq \binom{m}{n_y - 1},$$

where

$$f_i^t = d_t^+ / |\mathscr{A}_t^+ \bar{\lambda}|,\ \bar{\lambda} = \lambda / \|\lambda\|_2,$$

$$\lambda = C(I - A + LC)^{-1} G_i,$$

$$\mathscr{A}_t^+ = \frac{\mathbf{nX}(\tilde{H}^{\langle \gamma, \ldots, \eta \rangle})^T}{\|\mathbf{nX}(\tilde{H}^{\langle \gamma, \ldots, \eta \rangle})\|_2},\ d_t^+ = \sum_{j=1}^{m} |\mathscr{A}_i^+ \tilde{h}_j|,$$

$$\tilde{H} = \frac{1}{\|\lambda\|_2} \begin{bmatrix} 2H_z & 2\sqrt{\chi_n^2(1-\alpha)} S^{-1} \Lambda^{\frac{1}{2}} \end{bmatrix} \in \mathbb{R}^{n_y \times m}.$$

The index t *varies from 1 to* $\binom{m}{n_y-1}$ *and the indices* $\gamma, \ldots, \eta$ *are obtained by picking* $n_y - 1$ *out of* m *elements.* $\tilde{H}^{\langle \gamma, \ldots, \eta \rangle}$ *denotes matrix* $\tilde{H}$ *where the columns indexed by* $\gamma, \ldots, \eta$ *are removed.* $\tilde{h}_j$ *is the* j*th column of* $\tilde{H}$*.*

Please see the Appendix for the proof. □

Remark 5.3. Based on the above analysis results, we can implement the calculation of MDF for actuators with a confidence level of $1 - \alpha$. We would like to emphasize that the proposed method is also applicable to the calculation of MDF for sensors, and the whole mathematical derivation is similar to that of the actuator. Given the limited space, the detailed proofs and derivations are not listed here.

Remark 5.4. MDF is an important performance index of fault diagnosis and directly reflects the sensitivity of FD. From the design viewpoint, if MDF does not meet the design requirements under the Luenberger-observer framework, we may consider going back and tune the observer gains to further reduce MDF amplitude and thus increase FD sensitivity.

Remark 5.5. Note that, computing the magnitude of MDF for dynamic systems is a large topic. The current work mainly considers solving the MDF for time-invariant systems with additive actuator/sensor faults subject to hybrid Gaussian and bounded uncertainties. How to extend the current method to calculate the magnitude of MDF for complex nonlinear systems is still a problem worth in-depth study.

6. Illustrative examples

6.1. Case I: A two-link manipulator

In the first case, a two-link manipulator model used in Chen and Lin (2004) is considered. We choose the operating point $[\bar{q}_1\ \dot{\bar{q}}_1\ \bar{q}_2\ \dot{\bar{q}}_2]^T = [0.5\ 0.1\ 0.5\ 0.1]$ and $[\bar{\tau}_1\ \bar{\tau}_2]^T = [0.1\ 0.1]^T$ to linearize the original non-linear dynamics. Further, we take a sampling period $T_d = 1$ s and the related system parameters are obtained as

$$A = \begin{bmatrix} 1.000 & 1.000 & 0 & 0 \\ 1.465 & 1.210 & -2.229 & 0.127 \\ 0 & 0 & 1.000 & 1.000 \\ 14.809 & -0.631 & 2.983 & 0.706 \end{bmatrix},$$

$$B = \begin{bmatrix} 0 & 0.362 & 0 & -2.45 \\ 0 & -0.838 & 0 & 8.08 \end{bmatrix}^T,\ C = \begin{bmatrix} 1 & 0 & 0 & 0 \\ 0 & 0 & 1 & 0 \end{bmatrix}.$$

In this example, we consider four additive actuator faults $[f_1\ f_2\ f_3\ f_4]^T$ and two additive sensor faults $[s_1\ s_2]^T$, whose distribution matrices are respectively designed as

$$G = \begin{bmatrix} 0.815 & 0.632 & -1.958 & -0.357 \\ 0.906 & 0.098 & -0.965 & -0.485 \\ 0.127 & 0.279 & 1.158 & 1.800 \\ 0.913 & 0.547 & -0.971 & -0.942 \end{bmatrix},$$

$$P = \begin{bmatrix} 0.709 & -0.276 \\ 0.755 & -0.678 \end{bmatrix}.$$

Furthermore, the bounding zonotopes of the process disturbances $w_{z,k}$ and the measurement noises $v_{z,k}$ are designed as $\mathbf{W}_z = \{w \in \mathbb{R}^4 | \|w\|_\infty \leq 0.01\}$ and $\mathbf{V}_z = \{v \in \mathbb{R}^2 | \|v\|_\infty \leq 0.01\}$, whose distribution matrices E_z and F_z are respectively given as

$$E_z = \begin{bmatrix} 0.422 & 0.656 & 0.679 & 0.656 \\ 0.916 & 0.036 & 0.758 & 0.171 \\ 0.792 & 0.849 & 0.743 & 0.706 \\ 0.960 & 0.934 & 0.392 & 0.032 \end{bmatrix},\ F_z = \begin{bmatrix} 0.655 & 0.119 \\ 0.163 & 0.498 \end{bmatrix}.$$

The random vectors $w_{g,k}$ and $v_{g,k}$ follow the Gaussian distributions, and the related parameters are given as $w_g^c = [0\ 0\ 0\ 0]^T$, $v_g^c = [0\ 0]^T$, $Q_w = 0.01 I_4$, $Q_v = 0.01 I_2$. In addition, the coefficient matrices E_g and F_g are set as

$$E_g = \begin{bmatrix} 0.277 & 0.695 & 0.439 & 0.187 \\ 0.046 & 0.317 & 0.382 & 0.490 \\ 0.097 & 0.950 & 0.766 & 0.446 \\ 0.824 & 0.034 & 0.795 & 0.646 \end{bmatrix},\ F_g = \begin{bmatrix} 0.960 & 0.585 \\ 0.340 & 0.224 \end{bmatrix}.$$

Table 1
MDF for actuator and sensor faults.

Fault type	Value of MDF
Actuator fault f_1	0.4592
Actuator fault f_2	1.6880
Actuator fault f_3	0.4178
Actuator fault f_4	0.6558
Sensor fault s_1	0.1306
Sensor fault s_2	0.4230

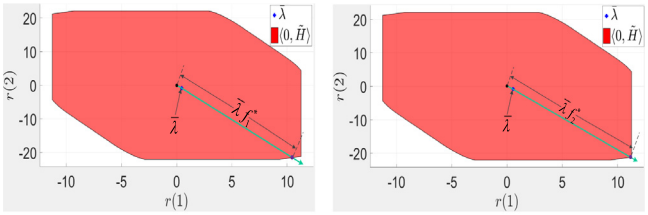

(a) Actuator fault f_1 (b) Actuator fault f_2

(c) Actuator fault f_3 (d) Actuator fault f_4

Fig. 1. Computation of MDF for actuator faults. (For interpretation of the references to color in this figure legend, the reader is referred to the web version of this article.)

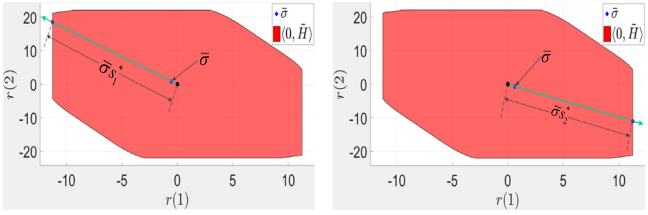

(a) Sensor fault s_1 (b) Sensor fualt s_2

Fig. 2. Computation of MDF for sensor faults.

The gain matrix L of the observer (2) is given as

$$L = \begin{bmatrix} 0.900 & 1.465 & 0 & 14.81 \\ 0 & -2.29 & 0.9 & 2.98 \end{bmatrix}^T.$$

The magnitudes of MDF for actuator and sensor faults are listed in Table 1. Regarding the computation of MDF for actuator faults, it is shown in Fig. 1. We take Fig. 1(a) as an example to illustrate the computation of MDF for the first actuator fault f_1. Based on the optimization problem (A.17), we need to find a minimal $f_1^*(f_1^* > 0)$ such that $\bar{\lambda} f_1^* \notin \langle 0, \tilde{H} \rangle$. In this case, f_1^* indicates the MDF for the first actuator fault f_1. In Fig. 1(a), the red region denotes the set $\langle 0, \tilde{H} \rangle$. The green arrow line represents the direction of the unit vector $\bar{\lambda}$. From a geometric point of view, f_1^* denotes the distance from the origin $\mathbf{0}$ to the boundary of $\langle 0, \tilde{H} \rangle$ along the direction vector $\bar{\lambda}$. Similar analysis is finished for the computation of MDF for the actuator faults f_2, f_3 and f_4 in Fig. 1(b), (c) and (d), respectively. Fig. 2 shows the computation of MDF for sensor faults s_1 and s_2 from the geometric point of view, which can be also analyzed similar to the actuator-fault case.

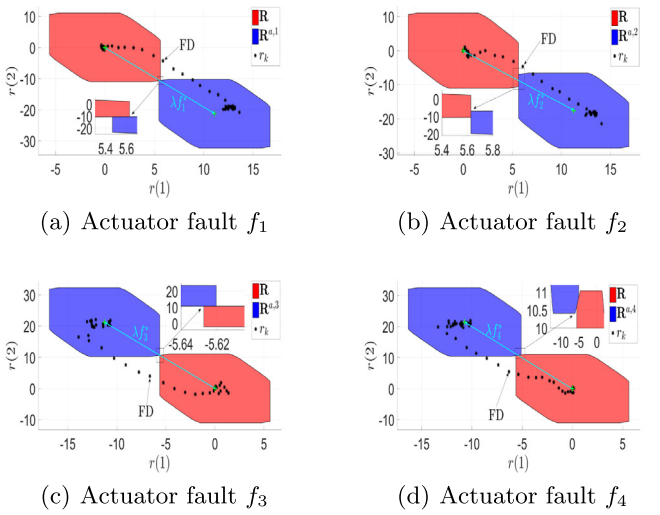

(a) Actuator fault f_1 (b) Actuator fault f_2

(c) Actuator fault f_3 (d) Actuator fault f_4

Fig. 3. Separation of residual sets and FD for actuator faults. (For interpretation of the references to color in this figure legend, the reader is referred to the web version of this article.)

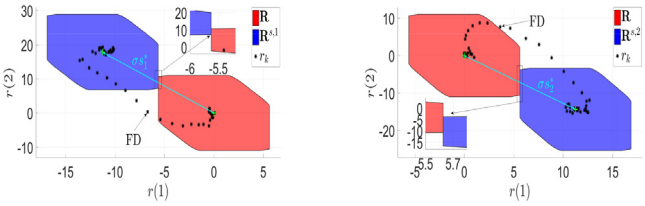

(a) Sensor fault s_1 (b) Sensor fault s_2

Fig. 4. Separation of residual sets and FD for sensor faults.

Fig. 3 shows the results on the separation of residual sets and FD for actuator faults. We take Fig. 3(a) as an example to illustrate the result of FD based on the separation of residual sets for the first actuator fault f_1. In Fig. 3(a), the red region denotes the healthy residual set $\mathbf{R}$, while the blue region represents the actuator-fault residual set $\mathbf{R}^{a,1}$ corresponding to the MDF f_1^*. It is shown that if the magnitude of occurred fault is equal to MDF f_1^*, the residual set $\mathbf{R}$ and the actuator-fault residual set $\mathbf{R}^{a,1}$ are just right separated from each other. The green arrow line between the centers of two residual sets represents the direction vector λf_1^*. We set the fault scenario as follows. From time instant $k = 1$ to $k = 10$, the system operates in healthy situation. While after $k = 10$, we inject the additive actuator fault f_1^* to the dynamics plant. It is shown that the residual signal r_k will leave the healthy residual set $\mathbf{R}$ and finally enter into the faulty residual set $\mathbf{R}^{a,1}$. Thus, FD is finished as long as the residual signal r_k goes out of the healthy residual set $\mathbf{R}$. Similar analysis can be also implemented for the residual set-separation based robust FD of the actuator faults f_2^*, f_3^* and f_4^*. Fig. 4 shows the results on the separation of residual sets and robust FD for sensor faults s_1^* and s_2^*, which can be also analyzed similar to the actuator-fault case.

6.2. Case II: A vehicle model

The second case study considers a linear vehicle model taken from Varrier et al. (2014) with fixed velocity to verify the effectiveness of the proposed MDF method. The related system matrices are given as

$$A = \begin{bmatrix} 0.7152 & 0.0220 \\ 0.2362 & 1.3891 \end{bmatrix}, B = \begin{bmatrix} 0.1175 \\ 0.3326 \end{bmatrix}, C = \begin{bmatrix} 1 & 0 \\ 0 & 1 \end{bmatrix},$$

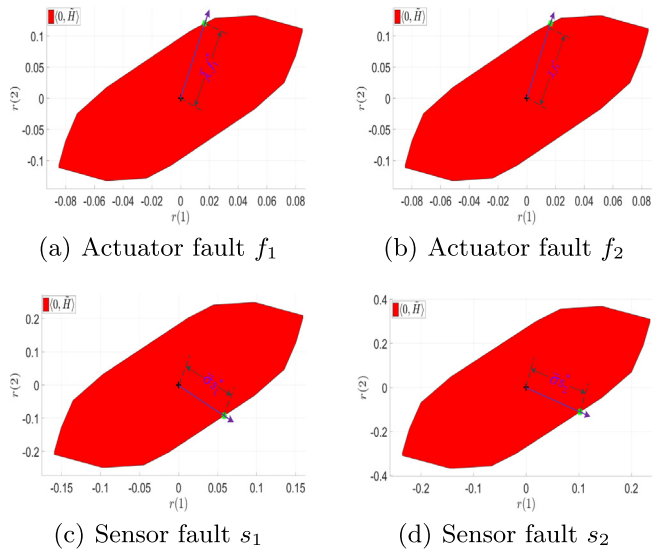

(a) Actuator fault f_1 (b) Actuator fault f_2

(c) Sensor fault s_1 (d) Sensor fault s_2

Fig. 5. Computation of MDF for actuator/sensor faults.

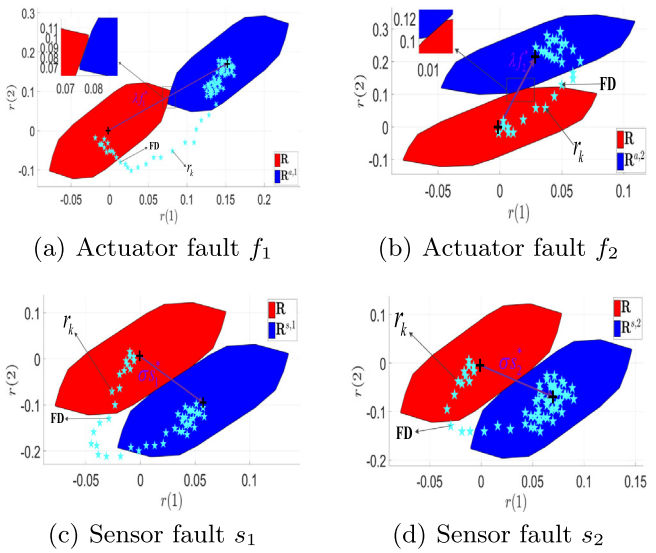

(a) Actuator fault f_1 (b) Actuator fault f_2

(c) Sensor fault s_1 (d) Sensor fault s_2

Fig. 6. Set-separation based FD for actuators/sensors. (For interpretation of the references to color in this figure legend, the reader is referred to the web version of this article.)

$$E_z = \begin{bmatrix} 0.6324 & 0.2785 \\ 0.0975 & 0.5469 \end{bmatrix}, E_g = \begin{bmatrix} 0.9575 & 0.1576 \\ 0.9649 & 0.9706 \end{bmatrix},$$

$$F_z = \begin{bmatrix} 0.4218 & 0.7922 \\ 0.9157 & 0.9595 \end{bmatrix}, F_g = \begin{bmatrix} 0.6557 & 0.8491 \\ 0.0357 & 0.9340 \end{bmatrix}.$$

The distribution matrices for actuator fault f_k and sensor fault s_k are given as

$$G = \begin{bmatrix} 0.8147 & 0.1270 \\ 0.9058 & 0.9134 \end{bmatrix}, P = \begin{bmatrix} 0.9572 & 0.8003 \\ 0.4854 & 0.1419 \end{bmatrix}.$$

Furthermore, the bounding zonotopes of $w_{z,k}$ and $v_{z,k}$ are designed as $\mathbf{W}_z = \{w \in \mathbb{R}^4 | \|w\|_\infty \leq 0.01\}$ and $\mathbf{V}_z = \{v \in \mathbb{R}^2 | \|v\|_\infty \leq 0.01\}$. The random vectors $w_{g,k}$ and $v_{g,k}$ follow the Gaussian distributions, and the related parameters are given by $w_g^c = [0,\ 0]^T$, $v_g^c = [0,\ 0]^T$, $Q_w = 0.001I_2$, $Q_v = 0.001I_2$. The gain matrix L is

$$L = \begin{bmatrix} 0.2152 & 0.0220 \\ 0.2362 & 0.8891 \end{bmatrix}.$$

Fig. 5 shows the computation results of MDF for actuator and sensor faults of the vehicle model based on $\bar{\lambda} f_i^* \notin \langle 0, \tilde{H} \rangle$ or $\bar{\sigma} s_i^* \notin \langle 0, \tilde{H} \rangle (i = 1, 2)$. Fig. 6 shows the results on residual set-separation based FD for actuator and sensor faults of the vehicle model. It is shown that the healthy residual set and the faulty residual set are just separated from each other when taking the MDF f_i^* and $s_i^* (i = 1, 2)$. The real residual signal r_k finally enters into the faulty residual set (the blue region) from the healthy residual set (the red region).

Finally, we make an in-depth comparative simulation between the current proposed method and the existed computational method of MDF dealing with the single bounded uncertainties in Tan, Olaru, Roman and Xu (2019). We set that the vehicle model operates in the healthy situation from the time instant $k = 1$ to time instant $k = 10$. After time instant $k = 10$, we inject the fault signals f_k or s_k into the system. Fig. 7 shows the results of fault detection and isolation (FDI) for the two actuator faults and two sensor faults. Fig. 8 further lists the values of MDF and the fault diagnosis time for the methods proposed in the context and Tan, Olaru, Roman and Xu (2019). It can be found that the current method has an advantage compared with the method in Tan, Olaru, Roman and Xu (2019) on the value of MDF and the diagnosis time. There are smaller values of MDF f_i^* and

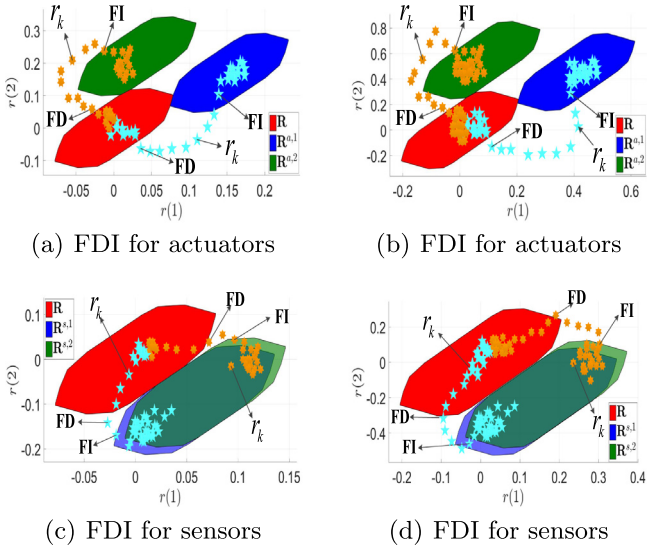

(a) FDI for actuators (b) FDI for actuators

(c) FDI for sensors (d) FDI for sensors

Fig. 7. Comparative results on FDI of actuators/sensors using the methods in the context and Tan, Olaru, Roman and Xu (2019).

$s_i^* (i = 1, 2)$ for the current method, which indicates a higher sensitivity of FD. The current method also has a shorter time delay for FD and fault isolation (FI).

7. Conclusions

This paper characterizes MDF for perturbed discrete-time LTI systems affected by additive faults using hybrid stochastic and deterministic approach. By considering the separation constraint of confidence residual sets in healthy and faulty situations, the computation of MDF is formulated a non-convex optimization problem. By exploiting the geometric property, the non-convex optimization problem is mathematically equivalent to compute the distance from the origin and the hyperplane of zonotope along the fixed direction, which can dramatically reduce the computational complexity.

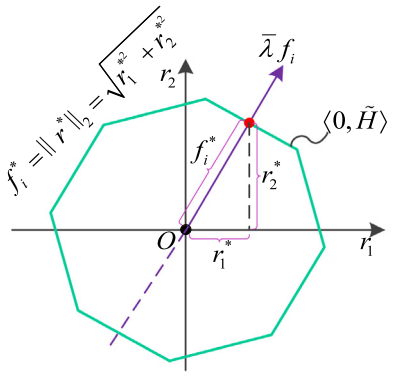

Fig. 8. Comparative results of MDF and fault diagnosis time in the context and Tan, Olaru, Roman and Xu (2019).

Acknowledgments

This work was supported by the National Natural Science Foundation of China (Grant No. 62103225, U21B6002), the National Key R&D Program of China (No. 2022YFB4701400/4701402) and Guangdong Basic and Applied Basic Research Foundation (No. 2022A1515010543).

Appendix. Proofs of Lemmas, Propositions and Theorems

A.1. Proof of Theorem 4.1

Proof. By iterating the dynamics of the state-estimation error vector $e_{g,k}$ from 0 to k, we can obtain

$$e_{g,k} = (A - LC)^k e_{g,0} + \alpha_k, \tag{A.1}$$

where $\alpha_k = \sum_{i=0}^{k-1}(A - LC)^i \gamma_{k-1-i}$ and $\gamma_{k-1-i} = E_g w_{g,k-1-i} - LF_g v_{g,k-1-i}$. Since $w_{g,k} \sim \mathcal{G}(w_g^c, Q_w)$, $v_{g,k} \sim \mathcal{G}(v_g^c, Q_v)$, $\forall k \in \mathbb{N}^+$, it follows

$$\gamma_{k-1-i} \sim \mathcal{G}(E_g w_g^c - LF_g v_g^c, E_g Q_w E_g^T + LF_g Q_v F_g^T L^T).$$

Considering $\alpha_k = \sum_{i=0}^{k-1}(A - LC)^i \gamma_{k-1-i}$, it follows

$$\alpha_k \sim \mathcal{G}(\beta_k, \Phi_k), \tag{A.2}$$

where

$$\beta_k = \sum_{i=0}^{k-1}(A - LC)^i (E_g w_g^c - LF_g v_g^c), \tag{A.3a}$$

$$\Phi_k = \sum_{i=0}^{k-1}(A - LC)^i (E_g Q_w E_g^T + LF_g Q_v F_g^T L^T) (A - LC)^{i^T}, \tag{A.3b}$$

Firstly, let us compute β_∞. By multiplying both sides of Eq. (A.3a) by $A - LC$, it follows

$$(A - LC)\beta_k = \sum_{i=1}^{k}(A - LC)^i (E_g w_g^c - LF_g v_g^c). \tag{A.4}$$

By subtracting (A.4) from (A.3a), we have

$$(I - A + LC)\beta_k = (E_g w_g^c - LF_g v_g^c) - (A - LC)^k \times (E_g w_g^c - LF_g v_g^c). \tag{A.5}$$

Considering $A - LC$ is a Schur matrix, we can obtain that as $k \to \infty$, $(A - LC)^k \to 0$. Thus, it follows (9a) based on (A.5).

Next, let us compute Φ_∞. Similarly, by left multiplying $A - LC$ and right multiplying $(A - LC)^T$ for both sides of Eq. (A.3b), it follows

$$(A - LC)\Phi_k(A - LC)^T = \sum_{i=1}^{k}(A - LC)^i (E_g Q_w E_g^T + LF_g Q_v F_g^T L^T)(A - LC)^{i^T}. \tag{A.6}$$

By subtracting (A.6) from (A.3b), it follows

$$\Phi_k - (A - LC)\Phi_k(A - LC)^T = (E_g Q_w E_g^T + LF_g Q_v F_g^T L^T) - (A - LC)^k (E_g Q_w E_g^T + LF_g Q_v F_g^T L^T)(A - LC)^{k^T}. \tag{A.7}$$

Considering the Schur stability of $A - LC$, by letting $k \to \infty$, we have

$$\Phi_\infty - (A - LC)\Phi_\infty(A - LC)^T = E_g Q_w E_g^T + LF_g Q_v F_g^T L^T. \tag{A.8}$$

Considering the vectorization of (A.8), it follows

$$(I - (A - LC) \otimes (A - LC))\mathbf{vec}(\Phi_\infty) = \mathbf{vec}(E_g Q_w E_g^T + LF_g Q_v F_g^T L^T). \tag{A.9}$$

Further, by matrixing (A.9), it follows (9b).

A.2. Proof of Theorem 5.1

Proof. Based on (10), it follows $r_{g,\infty} \sim \mathcal{G}(\mu, \mathcal{Q})$, where $\mu = C\beta_\infty + F_g v_g^c$ and $\mathcal{Q} = C\Phi_\infty C^T + F_g Q_v F_g^T$. By letting $\alpha \in [0,\ 1]$, based on Section 2.1, we obtain the confidence ellipsoid for the random vector $r_{g,\infty}$ as

$$\mathcal{E}_\alpha(\mu, \mathcal{Q}) \triangleq \{r | r \in \mathbb{R}^{n_y}, (r - \mu)^T \mathcal{Q}^{-1}(r - \mu) \le \chi^2_{n_y}(1 - \alpha)\}. \tag{A.10}$$

Since $\mathcal{Q}$ is a real symmetric matrix, there always exists an orthogonal transformation

$$\mathcal{Q} = S^T \Lambda S, \tag{A.11}$$

where S is an orthogonal matrix and Λ is a diagonal matrix. By substituting (A.11) into (A.10), it follows

$$\mathcal{E}_\alpha(\mu, \mathcal{Q}) = \{r | r \in \mathbb{R}^{n_y}, \frac{(r - \mu)^T S^T \Lambda^{-1} S(r - \mu)}{\chi^2_{n_y}(1 - \alpha)} \le 1\}. \tag{A.12}$$

Let us consider the linear mapping

$$\phi = \frac{1}{\sqrt{\chi^2_{n_y}(1 - \alpha)}} \Lambda^{-\frac{1}{2}} S(r - \mu). \tag{A.13}$$

Then the confidence ellipsoid (A.12) is transformed into a unit ball as

$$\mathbb{A}_2^{n_y}(1) = \{\phi \in \mathbb{R}^{n_y} | \phi^T \phi \le 1\}. \tag{A.14}$$

For the ball $\mathbb{A}_2^{n_y}(1)$, there always exist an outer-approximation unit box $\langle 0, I \rangle$ such that $\mathbb{A}_2^{n_y}(1) \subseteq \langle 0, I \rangle$. Further, based on the linear mapping (A.13), we consider the linear inverse mapping

$$r = \sqrt{\chi^2_{n_y}(1 - \alpha)} S^{-1} \Lambda^{\frac{1}{2}} \phi + \mu. \tag{A.15}$$

Based on the linear inverse mapping (A.15), the unit box $\langle 0, I \rangle$ is transformed into the zonotope

$$\mathbf{R}_g = \langle \mu, \sqrt{\chi^2_n(1 - \alpha)} S^{-1} \Lambda^{\frac{1}{2}} \rangle. \tag{A.16}$$

Obviously, the zonotope $\mathbf{R}_g$ should contain the confidence ellipsoid $\mathcal{E}_\alpha(\mu, \mathcal{Q})$, i.e., $\mathcal{E}_\alpha(\mu, \mathcal{Q}) \subseteq \mathbf{R}_g$. Thus, we have $\mathcal{P}(r_{g,\infty} \in \mathbf{R}_g) \ge \mathcal{P}(r_{g,\infty} \in \mathcal{E}_\alpha(\mu, \mathcal{Q})) = 1 - \alpha$.

A.3. Proof of Theorem 5.2

Proof. First prove (19a). Based on (8), we have $\mathcal{P}(r_{z,\infty} \in \mathbf{R}_z) = 1$. Considering $r_\infty = r_{z,\infty} + r_{g,\infty}$, it follows

$$\begin{aligned}\mathcal{P}(r_\infty \in \mathbf{R}) &= \mathcal{P}((r_{z,\infty} + r_{g,\infty}) \in \mathbf{R}) \\ &= \mathcal{P}((r_{z,\infty} + r_{g,\infty}) \in \mathbf{R}_z \oplus \mathbf{R}_g) \\ &\geq \mathcal{P}(r_{z,\infty} \in \mathbf{R}_z)\mathcal{P}(r_{g,\infty} \in \mathbf{R}_g) \\ &= \mathcal{P}(r_{g,\infty} \in \mathbf{R}_g) \geq 1 - \alpha.\end{aligned}$$

Next prove (19b). Similarly, considering $r_\infty^{a,i} = C(I-A+LC)^{-1}G_i f_i + r_{z,\infty} + r_{g,\infty}$, it follows

$$\begin{aligned}&\mathcal{P}(r_\infty^{a,i} \in \mathbf{R}^{a,i}) \\ &= \mathcal{P}((C(I - A + LC)^{-1}G_i f_i + r_{z,\infty} + r_{g,\infty}) \in \mathbf{R}^{a,i}) \\ &= \mathcal{P}((C(I - A + LC)^{-1}G_i f_i + r_{z,\infty} + r_{g,\infty}) \\ &\qquad \in \{C(I - A + LC)^{-1}G_i f_i\} \oplus \mathbf{R}_z \oplus \mathbf{R}_g) \\ &\geq \mathcal{P}(C(I - A + LC)^{-1}G_i f_i \in \{C(I - A + LC)^{-1}G_i f_i\}) \\ &\quad \mathcal{P}(r_{z,\infty} \in \mathbf{R}_z)\mathcal{P}(r_{g,\infty} \in \mathbf{R}_g) \\ &= \mathcal{P}(r_{g,\infty} \in \mathbf{R}_g) \geq 1 - \alpha.\end{aligned}$$

A.4. Proof of Theorem 5.3

Proof. Let us first consider the constraint $\mathbf{R} \cap \mathbf{R}^{a,i} = \emptyset$. Let $\lambda = C(I - A + LC)^{-1}G_i$, then

$$\begin{aligned}&\mathbf{R} \cap \mathbf{R}^{a,i} = \emptyset \\ \Longleftrightarrow\ &(\mathbf{R}_z \oplus \mathbf{R}_g) \cap (\{\lambda f_i\} \oplus \mathbf{R}_z \oplus \mathbf{R}_g) = \emptyset \\ \Longleftrightarrow\ &\mathbf{0} \notin \mathbf{R}_z \oplus \mathbf{R}_g \oplus \{-\lambda f_i\} \oplus (-\mathbf{R}_z) \oplus (-\mathbf{R}_g) \\ \Longleftrightarrow\ &\lambda f_i \notin \mathbf{R}_z \oplus \mathbf{R}_g \oplus (-\mathbf{R}_z) \oplus (-\mathbf{R}_g) \\ \Longleftrightarrow\ &\lambda f_i \notin \langle r_z^c, H_z\rangle \oplus \langle \mu, \sqrt{\chi_n^2(1-\alpha)}S^{-1}\Lambda^{\frac{1}{2}}\rangle \\ &\qquad \oplus \langle -r_z^c, H_z\rangle \oplus \langle -\mu, \sqrt{\chi_n^2(1-\alpha)}S^{-1}\Lambda^{\frac{1}{2}}\rangle \\ \Longleftrightarrow\ &\lambda f_i \notin \langle 0, 2H_z\rangle \oplus \langle 0, 2\sqrt{\chi_n^2(1-\alpha)}S^{-1}\Lambda^{\frac{1}{2}}\rangle \\ \Longleftrightarrow\ &\bar{\lambda} f_i \notin \langle 0, \tilde{H}\rangle,\end{aligned}$$

where the unit vector $\bar{\lambda} = \frac{\lambda}{\|\lambda\|_2}$ and $\tilde{H} = \frac{1}{\|\lambda\|_2}\left[2H_z \quad 2\sqrt{\chi_n^2(1-\alpha)}S^{-1}\Lambda^{\frac{1}{2}}\right] \in \mathbb{R}^{n_y \times m}$. Then, the optimization problem is changed to

$$\min_{f_i > 0} f_i \quad \text{s.t. } \bar{\lambda} f_i \notin \langle 0, \tilde{H}\rangle. \tag{A.17}$$

Regarding the optimization problem (A.17), it has an obvious geometrical significance as shown in Fig. A.1. We take the two-dimensional situation as a case. In Fig. A.1, $\bar{\lambda} f_i$ denotes a line passing through the origin O with the unit direction vector $\bar{\lambda}$, while $\langle 0, \tilde{H}\rangle$ represents the zonotope centered on the origin O. As f_i increases from 0 to infinity, $\bar{\lambda} f_i$ will also move from the origin O to the infinity along the direction $\bar{\lambda}$. During the above process, since $\langle 0, \tilde{H}\rangle$ is a closed zonotope contained on the origin O, there always exists an intersection (the red point in Fig. A.1) between the line $\bar{\lambda} f_i$ and the zonotope $\langle 0, \tilde{H}\rangle$. This point indicates the optimal solution f_i^* for the optimization problem (A.17). Therefore, solving the optimization problem (A.17) is equivalently transformed into searching the intersection point between the vector $\bar{\lambda} f_i$ and the zonotope $\langle 0, \tilde{H}\rangle$.

Based on Lemma 2.1, we have the half-space representation $\mathcal{H}(\langle 0, \tilde{H}\rangle) = \{r \in \mathbb{R}^{n_y} | \mathscr{A} r \leq d\}$ of $\langle 0, \tilde{H}\rangle$ as

$$\mathscr{A} = \begin{bmatrix} \mathscr{A}^+ \\ -\mathscr{A}^+ \end{bmatrix}, d = \begin{bmatrix} d^+ \\ d^+ \end{bmatrix}, \tag{A.18}$$

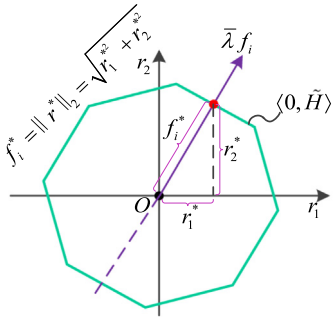

Fig. A.1. Geometrical illustration on the problem (A.17).

where

$$\mathscr{A}_t^+ = \frac{\mathbf{nX}(\tilde{H}^{\langle \gamma, \ldots, \eta\rangle})^T}{\|\mathbf{nX}(\tilde{H}^{\langle \gamma, \ldots, \eta\rangle})\|_2}, d_t^+ = \sum_{j=1}^{m} |\mathscr{A}_i^+ \tilde{h}_j|.$$

$\mathscr{A}_t^+$ denotes the tth row of $\mathscr{A}^+$, d_t^+ denotes the tth element of d^+ and $\tilde{h}_j$ denotes the jth column of $\tilde{H}$. The index t varies from 1 to $\binom{m}{n_y-1}$ and the indices $\gamma, \ldots, \eta$ are obtained by picking $n_y - 1$ out of m elements. $\tilde{H}^{\langle \gamma, \ldots, \eta\rangle}$ denotes matrix $\tilde{H}$ where the columns indexed by $\gamma, \ldots, \eta$ are removed.

Since the symmetry of $\mathcal{H}(\langle 0, \tilde{H}\rangle)$ regarding the origin O, we only need to consider the intersection point between the line $\bar{\lambda} f_i$ and the half zonotope $\mathcal{H}^+(\langle 0, \tilde{H}\rangle) = \{r \in \mathbb{R}^{n_y} | \mathscr{A}^+ r \leq d^+\}$. For each hyperplane $\{r \in \mathbb{R}^{n_y} | \mathscr{A}_t^+ r = d_t^+\}$, considering that the point $\bar{\lambda} f_i^t$ is in the hyperplane $\{r \in \mathbb{R}^{n_y} | \mathscr{A}_t^+ r = d_t^+\}$, it follows $\mathscr{A}_t^+ \bar{\lambda} f_i^t = d_t^+$. Further, we only consider the case of $f_i^t > 0$ and it can be obtained that $f_i^t = \frac{d_t^+}{|\mathscr{A}_t^+ \bar{\lambda}|}$. Therefore, the optimal f_i^* could be obtained by choosing the minimal value among the set $\{f_i^t\}$, $1 \leq t \leq \binom{m}{n_y-1}$.

References

Alamo, T., Bravo, J., & Camacho, E. (2005). Guaranteed state estimation by zonotopes. *Automatica*, *41*(6), 1035–1043.

Althoff, M. (2010). *Reachability analysis and its application to the safety assessment of autonomous cars* (Ph.D. thesis), Germany: Technical University of Munich.

Blanchini, F. (1999). Survey paper: Set invariance in control. *Automatica*, *35*(11), 1747–1767.

Blanke, M., Kinnaert, M., Lunze, J., & Staroswiecki, M. (2006). *Diagnosis and fault-tolerant control*. Berlin, Germany: Springer-Verlag.

Byod, S., & Vandenberghe, L. (2004). *Convex optimization*. Cambridge University Press.

Chabane, B. S. B., Maniu, S., Alamo, T., Camacho, E., & Dumur, D. (2014). Improved set-membership estimation approach based on zonotopes and ellipsoids. In *2014 European control conference* ECC, (pp. 993–998).

Chen, F., & Lin, J. (2004). Nonlinear backstepping design of robot manipulators with velocity estimation feedback. In *2004 5th Asian control conference, Vol. 1* (pp. 351–356).

Combastel, C. (2015). Zonotopes and kalman observers: Gain optimality under distinct uncertainty paradigms and robust convergence. *Automatica*, *55*, 265–273.

Gaßmann, V., & Althoff, M. (2020). Scalable zonotope-ellipsoid conversions using the euclidean zonotope norm. In *2020 American control conference* ACC, (pp. 4715–4721).

Kodakkadan, A., Pourasghar, M., Puig, V., Olaru, S., Ocampo-Martinez, C., & Reppa, V. (2017). Observer-based sensor fault detectability: About robust positive invariance approach and residual sensitivity. *IFAC-PapersOnLine*, *50*(1), 5041–5046.

Kofman, E., Doná, J. D., & Seron, M. (2012). Probabilistic set invariance and ultimate boundedness. *Automatica*, *48*(10), 2670–2676.

Kouvaritakis, B., Cannon, M., Raković, S. V., & Cheng, Q. (2010). Explicit use of probabilistic distributions in linear predictive control. *Automatica*, *46*(10), 1719–1724.

Li, X., & Zhou, K. (2009). A time domain approach to robust fault detection of linear time-varying systems. *Automatica*, *45*(1), 94–102.
Liu, J., Wang, J., & Yang, G. (2005). An LMI approach to minimum sensitivity analysis with application to fault detection. *Automatica*, *41*(11), 1995–2004.
Patton, R. (1997). Robustness in model-based fault diagnosis: the 1995 situation. *Annual Reviews in Control*, *21*, 103–123.
Pizzi, N., Kofman, E., Doná, J. D., & Seron, M. (2019). Actuator fault tolerant control based on probabilistic ultimate bounds. *ISA Transactions*, *84*, 20–30.
Pourasghar, M., Puig, V., & Ocampo-Martinez, C. (2016). Characterization of the minimum detectable fault of interval observers by using set-invariance theory. In *2016 3rd conference on control and fault-tolerant systems (SysTol)* (pp. 79–86).
Tan, J., Olaru, S., Roman, M., & Xu, F. (2019). Invariant-set based minimal detectable fault computation of discrete-time LPV systems with bounded uncertainties. In *58th IEEE conference on decision and control* CDC, (pp. 2940–2945).
Tan, J., Olaru, S., Roman, M., Xu, F., & Liang, B. (2019). Invariant set-based analysis of minimal detectable fault for discrete-time LPV systems with bounded uncertainties. *IEEE Access*, *7*, 152564–152575.
Tan, J., Olaru, S., Xu, F., Wang, X., & Liang, B. (2020). Optimal robust fault detection of discrete-time LPV systems with measurement error-affected scheduling variables combining ZKF and pQP. *International Journal of Robust and Nonlinear Control*, *30*(16), 6782–6802.
Tan, J., Xu, F., Olaru, S., Wang, X., & Liang, B. (2019). ZKF-based optimal robust fault estimation of descriptor LPVs systems with measurement error-affected scheduling variables. *ISA Transactions*, *94*, 119–134.
Varrier, S., Koenig, D., & Martinez, J. (2014). Robust fault detection for Uncertain Unknown Inputs LPV system. *Control Engineering Practice*, *22*, 125–134.
Zhang, X. (2016). *Matrix analysis and application*. Tsinghua University Press.
Zhang, Q. (2018). Adaptive Kalman filter for actuator fault diagnosis. *Automatica*, *93*(93), 333–342.
Zhang, Y., & Jiang, J. (2008). Bibliographical review on reconfigurable fault-tolerant control systems. *Annual Reviews in Control*, *32*(2), 229–252.

Junbo Tan received his Bachelor's degree in the Department of Management and Engineering from Nanjing University, Nanjing, P.R. China, in 2013, and his Master's degree in the Department of Automation from Tsinghua University, Beijing, P.R. China, in 2016, respectively. In 2020, he received his Ph.D. degree in the Navigation and Control Research Center, Tsinghua University. Currently, He is an Associate Researcher of Shenzhen International Graduate School, Tsinghua University. His research interests include Fault Diagnosis, Linear Parameter-Varying systems and Fault-tolerant Control.

Huailiang Zheng received the B.S., the M.S., and the Ph.D. degrees from the Department of Engineering Mechanics, Harbin Institute of Technology, Harbin, P.R. China, in 2013, 2015, and 2020, respectively. Currently, he is a Postdoctoral Researcher of Shenzhen International Graduate School, Tsinghua University. His research interests include Fault Diagnosis of Machinery System, Intelligent Fault Diagnosis Method, and Transfer Learning.

Deshan Meng received his B.E. degree in mechatronics engineering from the Liaoning University of Science and Technology, Anshan, P.R. China, in 2011, and his M.E. degree in mechatronics engineering from the Harbin Institute of Technology Shenzhen Graduate School, Shenzhen, P.R. China, in 2013, respectively. In 2017, he received his Ph.D. degree in the Department of Mechatronics and Automation, Harbin Institute of Technology Shenzhen Graduate School. Currently, he is an assistant professor with the School of Aeronautics and Astronautics, Sun Yat-sen University, Shenzhen, P.R. China. His research interests include Robot Dynamics and Control, Fault-tolerant Control.

Bo Yuan (Senior Member, IEEE) received the B.E. degree in computer science from the Nanjing University of Science and Technology, Nanjing, China, in 1998, and the M.Sc. and Ph.D. degrees in computer science from The University of Queensland (UQ), St Lucia, QLD, Australia, in 2002 and 2006, respectively. From 2006 to 2007, he was a Research Officer on a project funded by the Australian Research Council at UQ. From 2007 to 2021, he was a faculty member with the Division of Informatics, Shenzhen International Graduate School, Tsinghua University, Shenzhen, China. He is currently a research scientist with the Research Institute of Tsinghua University in Shenzhen. He is the inventor of 5 patents and the author of more than 120 papers in refereed international journals and conferences. His research interests include data science, evolutionary computation, and reinforcement learning.

Xueqian Wang received his Master's and Ph.D. degrees in Control Science and Engineering both from Harbin Institute of Technology (HIT), Harbin, P.R. China, in 2005 and 2010, respectively. From June 2010 to February 2014, he was a Postdoctoral Researcher at HIT. Since March 2014, he is currently professor and the leader of the Center for Artificial Intelligence and Robotics, Graduate School at Shenzhen, Tsinghua University. His research interests include Modeling, Control and Teleoperation of Robotic Systems.

Bin Liang received his Bachelor's degree and Master's degree both from the Honors College of Northwestern Polytechnical University, Xi'an, P.R. China, in 1989 and 1991, respectively, and his Ph.D. degree from the Department of Precision Instrument of Tsinghua University, Beijing, P.R. China, in 1994. From 1994 to 2007, he held his positions as a Postdoctoral Researcher, Associate Professor-level Researcher, Professor-level and Assistant Chief Engineer in the China Aerospace Science and Technology Corporation. Since 2007, he is currently a Professor in the Department of Automation of Tsinghua University. His research interests include Modelling and Control of Robotic Systems.